

Stability of wurtzite, unbuckled wurtzite, and rocksalt phases of SiC, GaN, InN, ZnO, and CdSe under loading of different triaxialities

K. Sarasamak,¹ A. J. Kulkarni,² M. Zhou,² and S. Limpijumnong¹

¹*School of Physics, Suranaree University of Technology and National Synchrotron Research Center, Nakhon Ratchasima 30000, Thailand*

²*The George W. Woodruff School of Mechanical Engineering, Georgia Institute of Technology, Atlanta, Georgia 30332-0405, USA*

(Received 29 August 2007; revised manuscript received 16 November 2007; published 7 January 2008)

First principles calculations are carried to study the structural stability of SiC, GaN, InN, ZnO, and CdSe which are found to transform from a fourfold coordinated *wurtzite* (WZ) structure under ambient conditions to two different crystalline structures under loading of different triaxialities. Under hydrostatic compression, transformation into a sixfold coordinated *rocksalt* (RS) structure occurs, and under uniaxial compression along the [0001] direction and uniaxial tension along the [01 $\bar{1}$ 0] crystalline direction (except SiC and GaN), transformation into a fivefold coordinated *unbuckled wurtzite* phase (HX) is observed. The lack of the WZ→HX transformation for SiC and GaN under uniaxial tension along the [01 $\bar{1}$ 0] direction is because for these two materials the tensile stress required for the enthalpy of HX to become lower than the enthalpy of WZ is higher than their corresponding ultimate tensile strength. Critical stress levels for the transformations are found to depend on the formation energies of the WZ, HX, and RS structures which in turn are related to the ionicity of each material. The transformations are a manifestation of the tension-compression response asymmetry of these materials.

DOI: [10.1103/PhysRevB.77.024104](https://doi.org/10.1103/PhysRevB.77.024104)

PACS number(s): 61.50.Ks, 62.20.-x, 64.70.K-

I. INTRODUCTION

One-to-one binary compounds obeying the octet rule (i.e., I-VII, II-VI, III-V, or IV-IV materials) are generally semiconductors or insulators. Although these type *AB* compounds have the same chemical formula units, their crystal structures under ambient conditions show significant variations with bond ionicity. While highly ionic compounds such as CsCl (I-VII) prefer dense crystal structures with a coordination number of 8 (CN=8), compounds such as NaCl (also I-VII) with lower degrees of ionicity gravitate toward the rocksalt (RS) structure (*Fm $\bar{3}$ m* space group) with CN=6. As the degree of ionicity decreases (shifting toward covalent bonding states), compounds such as ZnO (II-VI), GaN (III-V), and SiC (IV-IV) stabilize in wurtzite (WZ) (*P6 $_3$ mc*) structures with CN=4. In such covalent compounds, the valence electron counting (two electrons in each bond) is satisfied through the formation of four bonds for each atom. However, in compounds with higher degrees of ionicity such as CsCl and NaCl, the gain in cation-anion attractions leads to the formation of structures with higher CN. Nevertheless, bond ionicity should not be considered as the only factor in determining crystalline structures in such compounds since the assumption of a particular structure also depends on intrinsic factors such as composition, band structure, valence electrons, bonding states, and structural symmetries. Extrinsic factors such as loading and temperature also play significant roles.

Calculations and experiments have been carried out to study the structural stabilities of these materials. Over two decades ago, first principles calculations have been used to evaluate the formation energies of different crystalline structures (see, e.g., Refs. 1 and 2). X-ray diffraction experiments have been used to determine the natural occurring structures. Consequently, the stable crystalline structures under ambient conditions are well established (for a comprehensive review,

see Ref. 3). Furthermore, advances in experimental techniques, such as the use of intense and tunable x ray from synchrotron radiation, have also allowed x-ray diffraction analyses under external loading. For hydrostatic compression, it is observed that most materials with low CN structures (e.g., WZ and ZB) transform into a more compressed crystalline form with higher CN structures (e.g., RS).³⁻¹³ First principles and empirical potential calculations have yielded phase equilibrium pressures that are comparable but always lower than the transformation pressures measured from experiments.^{3,14-23} The higher experimental values are attributed to the existence of an energy barrier between the phases for each transformation. This finding is supported by, for example, the observation that critical pressure for the upward WZ→RS transformation is higher than the critical pressure for the downward RS→WZ transformation^{3,18} or the trapping of nanocrystallite ZnO in the RS phase under ambient condition after a high heat-high pressure treatment.²⁴ If there was no transformation barrier, the upward and downward transformations would occur at the same pressure and there would be no trapping of the metastable high pressure phase.

The recent synthesis of quasi-one-dimensional nanostructures such as nanowires, nanobelts, and nanorods of GaN, ZnO, and CdSe (see, e.g., Refs. 25 and 26) necessitates understanding the response of such materials to uniaxial loading. These nanostructures are single crystalline and nearly defect-free and, therefore, are endowed with high strengths and the ability to undergo large deformations without failure. Also, their high surface-to-volume ratios enhance atomic mobility and promote phase transformations under loading. A novel fivefold coordinated *unbuckled wurtzite* phase (HX) within the *P6 $_3$ /mmc* space group was observed in [01 $\bar{1}$ 0]-oriented ZnO nanowires under uniaxial tensile loading.^{27,28} The stability of this novel phase and the stabilities of WZ and RS phases of ZnO under uniaxial tension

along the $[01\bar{1}0]$ direction as well as hydrostatic compression were analyzed through enthalpy calculations. It is found that the HX structure cannot be stabilized by a hydrostatic pressure. Instead, both empirical potential based molecular dynamics (EP-MD) simulations and first principles calculations showed that transformation into the HX structure can occur under either tensile loading along the $[01\bar{1}0]$ direction or compressive loading along the $[0001]$ direction of sufficient magnitude. For this $WZ \rightarrow HX$ transformation, the uniaxial stress deforms the crystal in only one direction. Since the unit cell of HX is significantly shorter than the unit cell of WZ in the c or $[0001]$ direction (details later), either compression along the c direction or tension along the perpendicular $[01\bar{1}0]$ direction can cause the transformation. For compression along the c direction, the corresponding contribution to enthalpy by mechanical work is linearly proportional to $-\sigma_c \Delta c$, with σ_c and Δc being the compressive stress and the change in unit cell size in the c direction, respectively. For tension along the b direction, the corresponding contribution to enthalpy by mechanical work is linearly proportional to $-\sigma_b \Delta b$, with σ_b and Δb being the tensile stress and the change in unit cell size in the b direction, respectively. In contrast, for the $WZ \rightarrow RS$ transformation, the all around external pressure uniformly compresses the WZ crystal in all directions and causes it to collapse into the RS phase which has a lower equilibrium unit cell volume. The mechanical work contribution to enthalpy is $p\Delta V$, with p and ΔV being the external pressure and volume reduction, respectively. The discovery of the novel HX phase has subsequently been confirmed in $[0001]$ -oriented ZnO nanoplates²⁹ and nanowires.³⁰

To gain insight into the existence of the WZ, HX, and RS structures in materials with different ionicities, we analyze here the energetic favorability of these phases for ZnO and CdSe (groups II-VI), GaN and InN (III-V), and SiC (IV-IV) under uniaxial loading along the $[01\bar{1}0]$ and $[0001]$ crystal-line axes as well as under hydrostatic compression. The likelihood of transformations from WZ into HX or RS and the effort of load triaxialities on the transformations are analyzed.

II. CRYSTAL STRUCTURES

The natural form of the five materials studied is wurtzite, as shown in Fig. 1 (left column). This structure is quantified customarily by the lattice constant a , the c/a ratio, and the internal parameter u which specifies the relative distance along the c axis between the two hexagonal-close-packed cation and anion sublattices. To describe the HX and RS structures and the transformation from WZ to each of these phases, an extra lattice parameter b and an internal parameter v are introduced.^{19,20} v defines the horizontal distance along the b axis between the cation and anion sublattices. Out of the five parameters (a , b , c , u , and v) illustrated in Fig. 1, only the three external ones (a , b , and c) can be directly manipulated through applied loading. The two internal parameters (u and v) cannot be varied directly. These parameters are determined such that, for any given configuration,

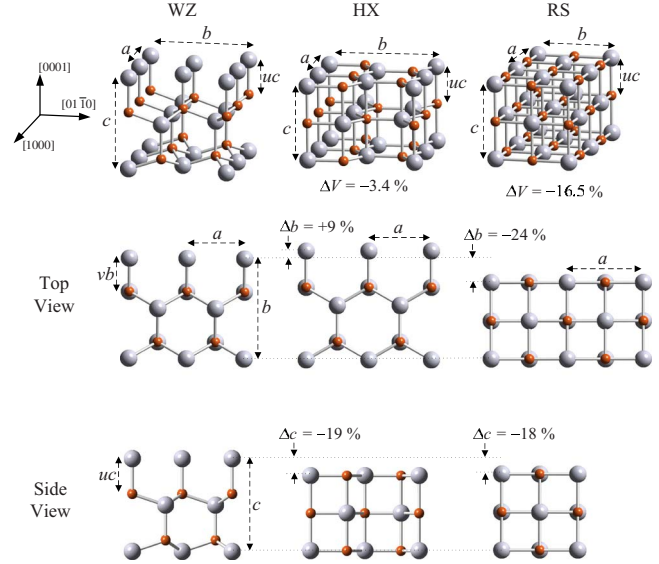


FIG. 1. (Color online) Schematic illustration of the WZ, HX, and RS structures: small spheres represent anions and large spheres represent cations. The middle and bottom rows show top view and side view, respectively. Parameters a , b , c , u , and v are indicated. For realistic rendering, the images shown are drawn to scale using parameters for ZnO at equilibrium conditions, i.e., ambient pressure for WZ, $\sigma = -\sigma_c^{\text{eq}}$ for HX, and $p = p^{\text{eq}}$ for RS. ΔV , Δb , and Δc are the percentage changes in V (volume), b , and c relative to the same quantities for WZ.

the net forces on all atoms in the unit cell vanish. An analysis of the variations of u with c/a and v with b/a can be found in Refs. 19 and 20. The three structures are significantly different, with $c/a \approx 1.63$ and $b/a \approx 1.73$ for WZ, $c/a \approx 1.20$ and $b/a \approx 1.73$ for HX, and $c/a \approx 1.00$ and $b/a \approx 1.00$ for RS. The ideal values of c/a , b/a , u , and v for WZ, HX, and RS under no load and zero temperature are listed in Table I. The c/a value for HX is obtained via enthalpy minimization. All other parameters are determined from the geometry of each structure, for instance, perfect tetrahedral coordination for WZ and perfect cubic for RS. Actual values of these parameters can deviate from those in the table, depending on the material, loading, and temperature.

III. COMPUTATIONAL METHOD

First principles calculations are carried out to evaluate the total energy of each material in its natural and deformed

TABLE I. Ideal lattice parameters for WZ, HX, and RS crystal-line structures.

Parameters	WZ	HX	RS
c/a	$\sqrt{8/3}=1.63$	1.20	1.00
u	$3/8=0.37$	0.50	0.50
b/a	$\sqrt{3}=1.73$	$\sqrt{3}=1.73$	1.00
v	$1/3=0.33$	$1/3=0.33$	0.50

states. The calculations are based on the density functional theory (DFT) with local density approximation (LDA) and ultrasoft pseudopotentials,³¹ as implemented in the VASP code.³² Test calculations have shown that generalize gradient approximations (GGAs) give the results that are qualitatively the same as LDA.³³ Zinc 3*d*, gallium 3*d*, indium 4*d*, and cadmium 4*d* electrons are treated as valence electrons. Cut-off energies for the plane wave expansion are 400 eV for ZnO, 180 eV for CdSe, 350 eV for nitrides, and 300 eV for SiC. The *k*-point sampling set is based on a $7 \times 7 \times 7$ division of the reciprocal unit cell based on the Monkhorst-Pack scheme³⁴ with the Γ point included, which gives approximately 100 inequivalent *k* points.

The stability of each crystal structure and compound can be determined by analyzing enthalpy as a function of *c/a* and *b/a*. The enthalpy per a *wurtzite unit cell* under uniaxial loading is

$$H(c/a, b/a) = E(c, b, a, u, v) - A_{jk} \sigma_i q_i, \quad (1)$$

where *E* is the formation energy per wurtzite unit cell, σ_i is the stress along the *i* direction, q_i is the lattice parameter in the *i* direction, A_{jk} is the cross section area of the unit cell perpendicular to the stress direction, and $A_{jk} \sigma_i q_i$ (summation not implied) is the external work. For tension along the *b* axis, $i=b$, $A_{ac}=ac/2$, and $q_b=b$, with σ_b being the tensile stress. For compression along the *c* axis, $i=c$, $A_{ab}=ab/2$, and $q_c=c$, with $-\sigma_c$ being the compressive stress. For hydrostatic compression, the enthalpy is

$$H(c/a, b/a) = E(c, b, a, u, v) + pV, \quad (2)$$

where *p* and $V=abc/2$ are the pressure and unit cell volume, respectively. Under ambient pressure, the enthalpy is equal to the internal formation energy. Note that a wurtzite unit cell contains two cation-anion pairs, i.e., 2 f.u. and occupy the volume $V=abc/2$.

For each *c/a* and *b/a* pair, the internal parameters *u* and *v* and the unit cell volume *V* are allowed to relax so that the configuration that yields the minimum *H* is obtained. For a given load condition, the minima on the enthalpy surface with *c/a* and *b/a* as the independent variables identify the corresponding stable and metastable structures. For the analyses at hand, the parameter ranges considered are [1.00, 1.63] for *c/a* and [1.00, 1.73] for *b/a*, with the increments of 0.05 for *c/a* and 0.10 for *b/a*. This meshing of the structural space results in approximately 170 strained configurations. For tensile loading along the *b* direction, additional configurations with *b/a* up to 2.30 are also investigated, increasing the number of total configurations to 200. Out of these 170 or 200 configurations, those around $(c/a, b/a) \approx (1.63, 1.73)$, $(1.2, 1.73)$, and $(1.00, 1.00)$ are more carefully analyzed since these three parameter sets define the neighborhoods of stable WZ, HX, and RS structures, respectively, for the given load condition.

For each strained configuration (each *c/a-b/a* pair), the energies associated with at least four different unit cell volumes are calculated. An equation of state (energy-volume relation) is obtained by a third-degree polynomial fit. Under loading, the volume that minimizes *H* is not the same as the volume that minimizes *E*. The equation of state allows the

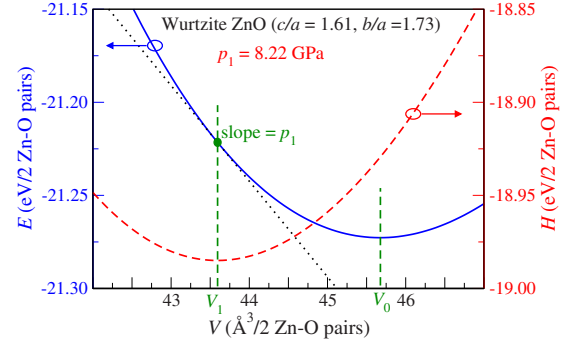


FIG. 2. (Color online) Energy (solid curve) and enthalpy (dashed curve) as functions of volume for wurtzite ($c/a=1.61$ and $b/a=1.73$) ZnO. At hydrostatic pressure $p_1=8.22$ GPa, the volume that minimizes enthalpy (V_1) is smaller than the volume at ambient pressure (V_0).

minimum enthalpy for each combination of *c/a-b/a* pair and loading condition to be obtained. As an illustration, the energy and enthalpy are shown in Fig. 2 as functions of volume for WZ ZnO ($c/a=1.61$ and $b/a=1.73$) under hydrostatic pressure. At ambient pressure ($p \approx 0$), the energy and enthalpy are equal and the minimum enthalpy is equal to $E(V_0)$, with V_0 being the equilibrium volume of WZ in a stress-free state. At $p=p_1$, the minimum enthalpy occurs at $V=V_1$ for which $dE/dV=-p_1$.

IV. RESULTS AND DISCUSSIONS

A. Ambient conditions (stress-free state)

Figure 3(a) shows the energy (or enthalpy at zero external loading) landscape for ZnO. The global minimum occurs at the wurtzite structure with $(c/a, b/a)=(1.61, 1.73)$. The sections of the surface along $b/a=1.73$ (solid line) and 1.00 (dash line) are shown in Fig. 3(b). By virtue of symmetry, *b/a* is fixed at $\sqrt{3}(\approx 1.73)$ for WZ and HX and at 1.00 for RS. Clearly, in stress-free state, WZ is the most stable structure with the lowest energy, HX has higher energy and is not stable (no local minimum), and the RS structure is metastable with a high energy. For CdSe, GaN, InN, and SiC, the shapes of the energy landscapes (not shown but can be found online³⁵) are similar to that of ZnO. Their two-dimensional (2D) sections at $b/a=1.73$ and 1.00 are shown in Fig. 4. The energy difference (see Ref. 36) between HX and WZ ($\Delta E^{\text{HX-WZ}}$) and that between RS and WZ ($\Delta E^{\text{RS-WZ}}$) are tabulated in Table II. The energies of the three phases for all compounds except CdSe follow the order of $E^{\text{RS}} > E^{\text{HX}} > E^{\text{WZ}}$. For CdSe, $E^{\text{RS}} < E^{\text{HX}}$. This exception can be attributed to the fact that for compounds such as CdSe with high ionicity, the energy differences between RS, HX, and WZ are relatively small. Under this situation, other effects, such as energy cost for bond distortions, can affect the ordering in energies.

There are significant variations of $\Delta E^{\text{HX-WZ}}$ or $\Delta E^{\text{RS-WZ}}$ among the materials, partly reflecting differences in the ionicity. Several indices are available to describe the ionicity of materials. Although LDA calculation is sometimes believed

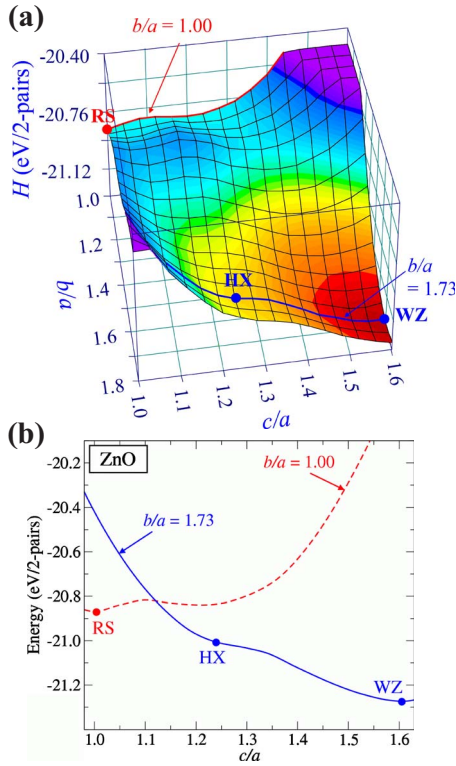


FIG. 3. (Color online) (a) Energy (E) (or enthalpy H under zero external loading) landscape for ZnO (in eV per wurtzite unit cell which contains two cation-anion pairs or 2 f.u.). Each point on the surface represents the minimum energy for a given combination of c/a and b/a . To arrive at the minimum, u , v , and V are allowed to relax while a , b , and c are kept constant. Energy levels above -20.50 eV are truncated as they are not of interest in the discussions here. (b) 2D sections of the energy surface for $b/a=1.73$ (solid line) and 1.00 (dashed line).

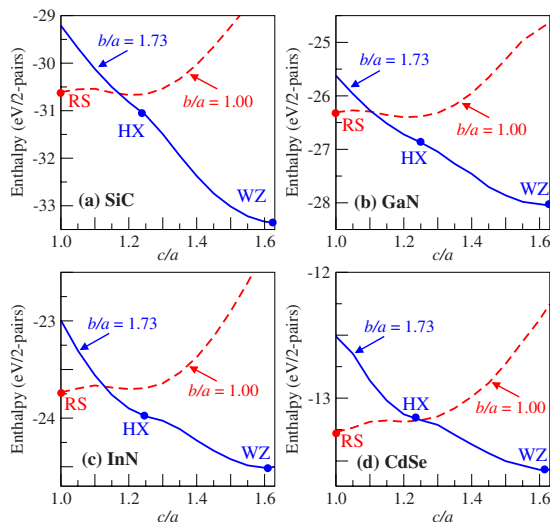


FIG. 4. (Color online) 2D sections of (a) SiC, (b) GaN, (c) InN, and (d) CdSe energy surfaces (Ref. 35) for $b/a=1.73$ (solid lines) and 1.00 (dashed lines).

TABLE II. Energy difference (eV/2 pairs) between HX (or RS) and the WZ structure. The Phillips ionicity parameters (f_i) are also listed. (Ref. 37).

Compounds	Phillips' f_i	$E^{\text{HX}} - E^{\text{WZ}}$ (eV)	$E^{\text{RS}} - E^{\text{WZ}}$ (eV)
SiC	0.177	2.53	2.74
GaN	0.500	1.32	1.74
InN	0.578	0.61	0.78
ZnO	0.616	0.26	0.41
CdSe	0.699	0.44	0.30

to slightly overestimate the ionicity in materials, the trend of ionicity between materials should be qualitatively correct. Therefore, Phillips' ionic scale (f_i),³⁷ which has the range between 0 (the least ionic) and 1 (the most ionic), is used here by choice. The values of f_i for the compounds studied here are listed in Table II.³⁷ The variations of $\Delta E^{\text{HX-WZ}}$ and $\Delta E^{\text{RS-WZ}}$ with f_i are shown in Fig. 5. For RS, $\Delta E^{\text{RS-WZ}}$ (solid line) decreases monotonically as f_i increases. For HX, $\Delta E^{\text{HX-WZ}}$ (dash line) decreases monotonically with f_i (except for CdSe). This is expected because compounds with higher levels of ionicity can significantly lower their energies through increases in CN. While ionicity is not the only factor that determines the relative stability of crystal structures, it clearly affects the stability of structures. For covalent compounds (e.g., SiC and GaN), the structure with fourfold coordination is highly favored, resulting in large differences between the formation energies of RS (sixfold) and WZ (fourfold) and between the formation energies of HX (fivefold) and WZ. On the other hand, for compounds with higher levels of ionicity, the differences in formation energies among RS, HX, and WZ are lower. In this paper, only ionic compounds that have fourfold coordinated structures (WZ) under ambient conditions are considered.

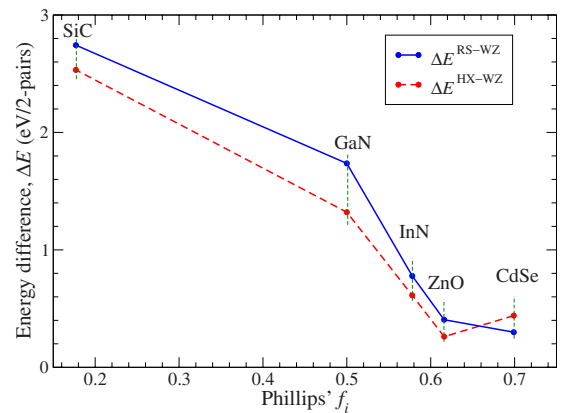


FIG. 5. (Color online) Correlation between the formation energy differences (ΔE) and the ionicity as quantified by Phillips' f_i for SiC, GaN, InN, ZnO, and CdSe. $\Delta E^{\text{RS-WZ}}$ is shown in solid line and $\Delta E^{\text{HX-WZ}}$ is shown in dash line. For all compounds, WZ has the lowest energy and RS has the highest energy, except for CdSe whose RS phase has a slightly lower energy than its HX phase.

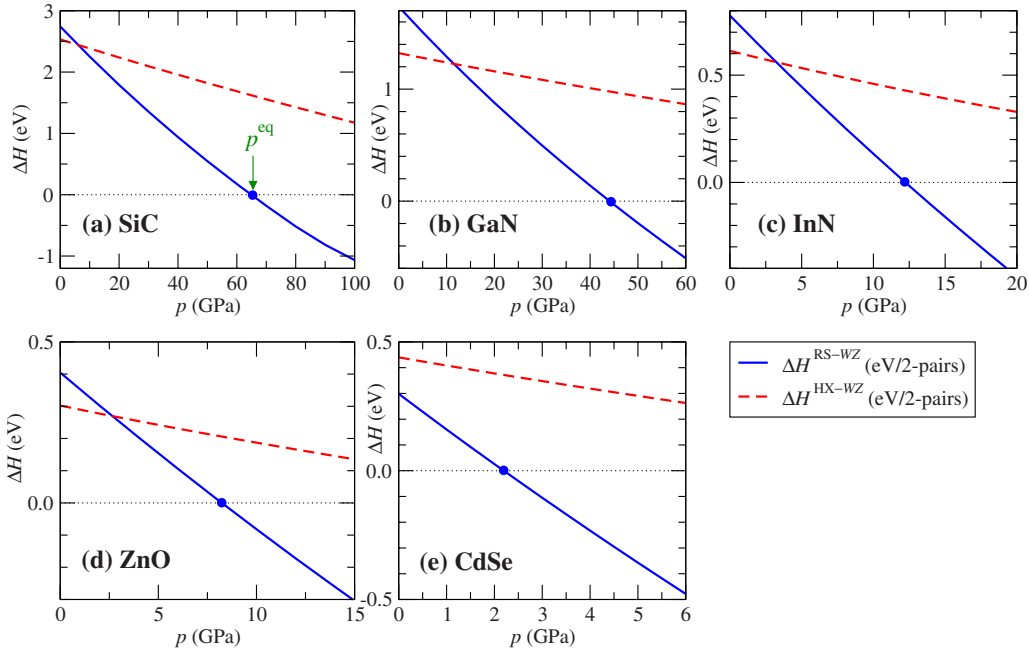


FIG. 6. (Color online) Enthalpy differences (ΔH), in the unit of eV/2 pairs, between RS and WZ (solid line) and HX and WZ (dashed line) as a function of hydrostatic pressure for (a) SiC, (b) GaN, (c) InN, (d) ZnO, and (e) CdSe. As the pressure reaches the equilibrium value (p^{eq} , indicated by solid dots), the enthalpies for RS and WZ become equal. Above p^{eq} , RS is more stable. Note that HX is never stable under hydrostatic loading.

B. Hydrostatic compression

Sufficiently high pressures can cause the WZ structure to collapse into the denser RS phase. As shown in Fig. 1, the volume of the RS structure is $\sim 17\%$ smaller than the volume of the WZ structure ($\Delta V \approx -0.17V_0$, with V_0 being the equilibrium volume of WZ). For a given constant pressure p , the difference in contributions to enthalpy by mechanical work between RS and WZ is approximately $p\Delta V$ (neglecting the difference in bulk moduli of the two phases). If p is sufficiently high, mechanical work can overcome the formation energy difference, driving the transformation forward. Figure 6 shows $\Delta H^{\text{RS-WZ}} = H^{\text{RS}} - H^{\text{WZ}}$ and $\Delta H^{\text{HX-WZ}} = H^{\text{HX}} - H^{\text{WZ}}$ as functions of p for the five compounds studied. The rather linear trends confirm that the bulk moduli of the WZ, HX, and RS phases are quite comparable. The slight deviation from linearity of $\Delta H^{\text{RS-WZ}}$ reflects the fact that the bulk modulus of RS is somewhat higher (approximately 25%) than that of WZ. Note that the slope of the $\Delta H^{\text{RS-WZ}}$ line is approximately five times that of the $\Delta H^{\text{HX-WZ}}$ line, consistent with the fact that the volume decrease associated with the WZ \rightarrow RS transformation (17%) is approximately five times of that associated with the WZ \rightarrow HX transformation (3.6%).

The equilibrium pressure p^{eq} between the WZ and RS structures (the pressure at which the enthalpies of RS and WZ become equal) can be obtained by examining the enthalpy surfaces at several pressures. This pressure is identified with the intercept of the enthalpy curve with the horizontal axis in Fig. 6. The enthalpy surfaces of all five materials at their equilibrium pressure p^{eq} are qualitatively the same (not shown here but can be found online³⁵). There-

fore, we choose to present only the enthalpy surface for InN in Fig. 7(a). The corresponding 2D section is shown in Fig. 7(b). At $p < p^{\text{eq}}$, WZ has the lowest enthalpy. As p is increased above p^{eq} , RS has a lower enthalpy than WZ. p^{eq} depends strongly on the ionicity of the compound. This is expected because the initial energy difference between WZ and RS ($\Delta E^{\text{RS-WZ}} = E^{\text{RS}} - E^{\text{WZ}}$) depends on the ionicity of the material (from $\Delta E^{\text{RS-WZ}} = 2.74$ eV for SiC to 0.30 eV for CdSe). SiC has the highest $\Delta E^{\text{RS-WZ}}$ and therefore the highest p^{eq} (64.9 GPa). CdSe has the lowest $\Delta E^{\text{RS-WZ}}$ and therefore the lowest p^{eq} (2.2 GPa). The equilibrium pressures of the five materials are listed in Table III. Our calculated equilibrium pressures are in good agreement with other calculated results in general (see Table III). To compare with experiments, one should not directly compare the calculated equilibrium pressure with either the critical pressures of the upward or downward WZ to RS transformations. This is because there is a transformation barrier between the two phases that causes the upward critical pressure to be higher (and the downward critical pressure to be lower) than the equilibrium pressure.^{3,18} The averages between the upward and downward critical pressures, shown as p_t in Table III, are shown as an approximate experimental equilibrium pressures and are in good agreement with the calculated equilibrium pressures.

To gain insight on the transformation enthalpy barrier, we extracted (from the plots) the *homogeneous* transformation barrier (in the unit of eV/2 pairs) of these five materials and tabulated in Table III using square brackets. The barrier for ZnO of 0.30 eV/2 pairs is the same as Limpijumnong and Jungthawan have previously reported.¹⁸ The barriers for SiC and GaN of 1.26 and 0.76 eV/2 pairs are in good agreement

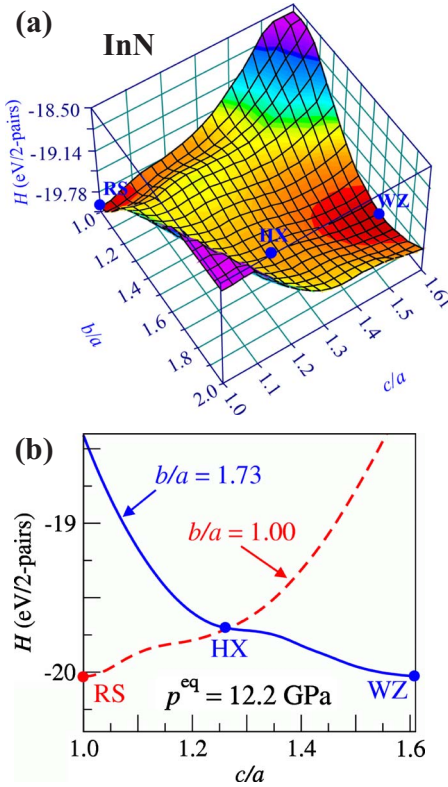


FIG. 7. (Color online) (a) Enthalpy surface maps (in eV/2 pairs) for InN at its RS-WZ equilibrium pressures, $p^{\text{eq}}=12.2$ GPa. (b) 2D sections of the enthalpy surface for $b/a=1.73$ (solid line) and 1.00 (dashed line).

with the calculated values reported by Miao and Lambrecht³⁸ (for SiC) of 1.2 eV/2 pairs and by Limpijumnong and Lambrecht²⁰ (for GaN) of 0.9 eV/2 pairs. We can see that the magnitude of the barrier increases with the zero pressure energy difference between phases ($\Delta E^{\text{RS-WZ}}$), hence the ionicity. The detailed investigation of the barriers will be a subject of further study on more materials in the future.

Figure 8 shows the variation of equilibrium pressure with the initial energy difference. An approximately linear dependence of p^{eq} on $\Delta E^{\text{RS-WZ}}$ is seen. The linear fit gives

$$p^{\text{eq}} \approx 25.97(\Delta E^{\text{RS-WZ}}) - 4.68. \quad (3)$$

The units of p^{eq} and $\Delta E^{\text{RS-WZ}}$ are in GPa and eV/2 pairs, respectively. This approximate universal relationship can be used to estimate the difference in the formation energy of the RS and WZ phases when the equilibrium pressure is known or vice versa.

Figure 6 also shows that the $\Delta H^{\text{HX-WZ}}$ line never intercepts the horizontal axis for all five materials over the pressure range analyzed. Obviously, HX is not a thermodynamically stable structure under hydrostatic compression and the WZ \rightarrow HX transformation does not occur for such conditions.

C. Uniaxial compression along the [0001] direction

Figure 1 shows that HX has a lattice constant c significantly shorter ($\sim 19\%$) than that of WZ in the [0001] direc-

tion. This difference allows WZ to transform into HX via compression in the c direction. Under constant compressive stress $-\sigma_c$ (negative sign indicates compression), the mechanical contribution to the enthalpy difference between WZ and HX is $-A_{ab}\sigma_c\Delta c$, where $\Delta c \approx -0.19c$. A sufficiently high $-\sigma_c$ would allow mechanical work to offset the energy difference between HX and WZ, affecting the transformation into the HX structure. The shapes of the enthalpy surfaces for SiC, GaN, InN, and ZnO at their respective equilibrium compressive stress $-\sigma_c^{\text{eq}}$ are qualitatively the same (not shown here but can be found online³⁵). Therefore, we choose

Material	p^{eq} (GPa)		p_t (GPa)	$-\sigma_c^{\text{eq}}$ and σ_b^{eq} (GPa)	
	(Present)	(Other)	(Expt.)	$-\sigma_c^{\text{eq}}$	σ_b^{eq}
SiC	64.9[1.26]	60, ^a 66.6, ^b 66, ^c 92 ^d	67.5 ^e	60.5	
GaN	44.1[0.76]	51.8, ^f 42.9 ^g	52.2, ^h 31 ⁱ	30.5	
InN	12.2[0.51]	21.6, ^f 11.1 ^g	10, ^j 12.1 ^h	9.6	14.7
ZnO	8.2[0.30]	6.6, ^k 9.3, ^l 8.0 ^m	5.5, ⁿ 8.5 ^o	6.0	10.8
CdSe	2.2[0.40]	2.5 ^p	2.1 ^q	3.8	5.8

^aDFT (GGA) calculations by Miao and Lambrecht (Ref. 41).

^bDFT (LDA) calculations (of zincblende to RS) by Karch *et al.* (Ref. 17).

^cDFT (LDA) calculations (of zincblende to RS) by Chang and Cohen (Ref. 42).

^dDFT (B3Lyp) calculations (of zincblende to RS) by Catti (Ref. 43).

^eSynchrotron angle dispersive x-ray diffraction (ADX) experiment by Yoshida *et al.* (Ref. 10).

^fDFT (LDA) calculations by Christensen and Gorczyca (Ref. 14).

^gDFT (LDA) calculations by Serrano *et al.* (Ref. 44).

^hADX experiment by Ueno *et al.* (Ref. 6).

ⁱSynchrotron energy-dispersive x-ray diffraction (EDX) by Xia *et al.* (Ref. 8).

^jSynchrotron EDX experiment by Xia *et al.* (Ref. 9).

^kDFT (LDA) calculations by Jaffe *et al.* (Ref. 16).

^lDFT (GGA) calculations by Jaffe *et al.* (Ref. 16).

^mDFT (GGA) calculations by Ahuja *et al.* (Ref. 45).

ⁿSynchrotron EDX experiment by Desgreniers. (Ref. 5).

^oSynchrotron EDX experiment by Recio *et al.* (Ref. 46).

^pDFT (LDA) calculations by Côté *et al.* (Ref. 23).

^qEDX experiment by Cline and Stephens (Ref. 4).

tion. This difference allows WZ to transform into HX via compression in the c direction. Under constant compressive stress $-\sigma_c$ (negative sign indicates compression), the mechanical contribution to the enthalpy difference between WZ and HX is $-A_{ab}\sigma_c\Delta c$, where $\Delta c \approx -0.19c$. A sufficiently high $-\sigma_c$ would allow mechanical work to offset the energy difference between HX and WZ, affecting the transformation into the HX structure. The shapes of the enthalpy surfaces for SiC, GaN, InN, and ZnO at their respective equilibrium compressive stress $-\sigma_c^{\text{eq}}$ are qualitatively the same (not shown here but can be found online³⁵). Therefore, we choose

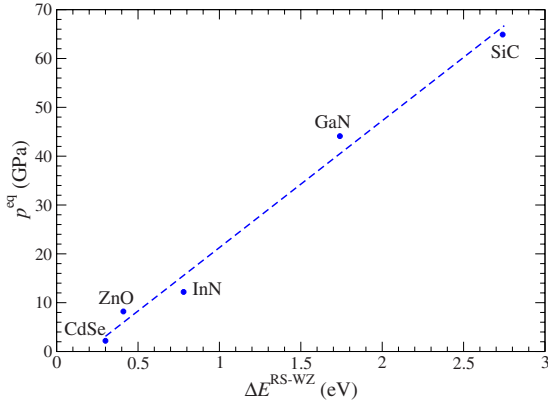


FIG. 8. (Color online) Correlation between equilibrium hydrostatic pressure (p^{eq}) and the difference in energy (ΔE) between the RS and WZ phases of the five materials. p^{eq} is the pressure at which the WZ and RS structures are in equilibrium, as illustrated in Fig. 6 and tabulated in Table III. The energy difference $\Delta E = E^{\text{RS}} - E^{\text{WZ}}$ is calculated under the conditions of zero external loading and is tabulated in Table II.

to present the enthalpy surface for InN with a 2D section plot in Fig. 9(a). The stability of the HX phase can be better analyzed through the enthalpy difference $\Delta H^{\text{HX-WZ}} = H^{\text{HX}} - H^{\text{WZ}}$ as a function of the compressive stress along the c direction (dashed lines, Fig. 10). If the elastic moduli of HX and WZ along the c direction are assumed to be equal, ΔH would vary linearly with $-\sigma_c$ with an approximate slope of $A_{ab}\Delta c \approx -0.19(abc/2) \approx -0.19V$. Figure 10 also shows the enthalpy difference between RS and WZ, $\Delta H^{\text{RS-WZ}} = H^{\text{RS}} - H^{\text{WZ}}$ (solid lines). Note that $\Delta H^{\text{HX-WZ}}$ and $\Delta H^{\text{RS-WZ}}$

show similar trends, with similar slopes. This is because for the $\text{WZ} \rightarrow \text{RS}$ transformation, $\Delta c/c \approx 18\%$, while for the $\text{WZ} \rightarrow \text{HX}$ transformation, $\Delta c/c \approx 19\%$.

For all materials except CdSe, $\Delta H^{\text{HX-WZ}}$ is always lower than $\Delta H^{\text{RS-WZ}}$, indicating that HX is more stable than RS under compression in the c direction. For CdSe, where initially (i.e., under no load condition) the RS phase has a slightly lower energy than HX, $\Delta H^{\text{RS-WZ}}$ is always lower than $\Delta H^{\text{HX-WZ}}$, indicating that RS is the preferred structure over HX under uniaxial compression along the $[0001]$ direction as well as under hydrostatic compression. As a result, the the enthalpy surface at $-\sigma_c^{\text{eq}}$ of CdSe [Fig. 9(b)] is qualitatively different from those of the other four materials [represented by Fig. 9(a)], i.e., the RS phase has lower enthalpy. The equilibrium stress for the transformation ($-\sigma_c^{\text{eq}}$) of each material is shown in Fig. 10. Below $-\sigma_c^{\text{eq}}$, WZ phase is stable. Above $-\sigma_c^{\text{eq}}$, HX is stable (RS for CdSe). The values of $-\sigma_c^{\text{eq}}$ depend on the initial energy difference (ΔE) between WZ and HX and are listed in Table III. For SiC, $\Delta E = E^{\text{HX}} - E^{\text{WZ}} = 2.53$ eV, the stress required to cause the $\text{HX} \rightarrow \text{WZ}$ transformation is high ($-\sigma_c^{\text{eq}} = 60.5$ GPa). On the other hand, for ZnO, $\Delta E = 0.26$ eV and $-\sigma_c^{\text{eq}} = 6.0$ GPa which is only 1/10 of the stress level required for SiC. This linear trend is clearly seen in Fig. 11 which shows $-\sigma_c^{\text{eq}}$ as a function of ΔE for the materials analyzed. The linear fit gives

$$-\sigma_c^{\text{eq}} \approx 25.72(\Delta E^{\text{HX-WZ}}) - 4.56. \quad (4)$$

The coefficients in the equation are based on the units of $-\sigma_c^{\text{eq}}$ and $\Delta E^{\text{HX-WZ}}$ in GPa and eV/2 pairs, respectively. The similarity in the numerical values of coefficients of Eqs. (4) and (3) is fortuitous. Note that the WZ-HX homogeneous transformation enthalpy barrier is significantly lower than that of WZ-RS, i.e., always less than 0.1 eV/2 pairs for all materials studied except SiC. However, for SiC, the barrier is only slightly higher, i.e., 0.13 eV/2 pairs.

D. Uniaxial tension along the $[01\bar{1}0]$ direction

The HX structure also has a longer dimension in the $[01\bar{1}0]$ direction compared to the WZ structure (longer by approximately 9%, see Fig. 1, middle column). This difference allows WZ to transform into HX via tension in the b ($[01\bar{1}0]$) direction. Note that the difference in b between the two structures is only about half of the difference in c . Accordingly, the mechanical enthalpy contribution $A_{ac}\sigma_b\Delta b$ is roughly half of the case of c compression for the comparable stress magnitude. Only three (InN, ZnO, and CdSe) out of the five materials studied have a local minimum corresponding to the HX structure under tensile loading along the b direction. We choose to present the enthalpy surfaces for InN (those for ZnO and CdSe can be found online³⁵) at the equilibrium tensile stress σ_b^{eq} [Fig. 12(a)] with its 2D section plot [Fig. 12(b)]. The plot³⁵ between the enthalpy differences $\Delta H^{\text{HX-WZ}} = H^{\text{HX}} - H^{\text{WZ}}$ as functions of tensile stress σ_b are similar to the compressive stress case. The equilibrium tensile stress σ_b^{eq} (14.7, 10.8, and 5.8 GPa for InN, ZnO, and CdSe, respectively) is approximately twice the equilibrium compressive stress $-\sigma_c^{\text{eq}}$ for the c direction. EP-MD simula-

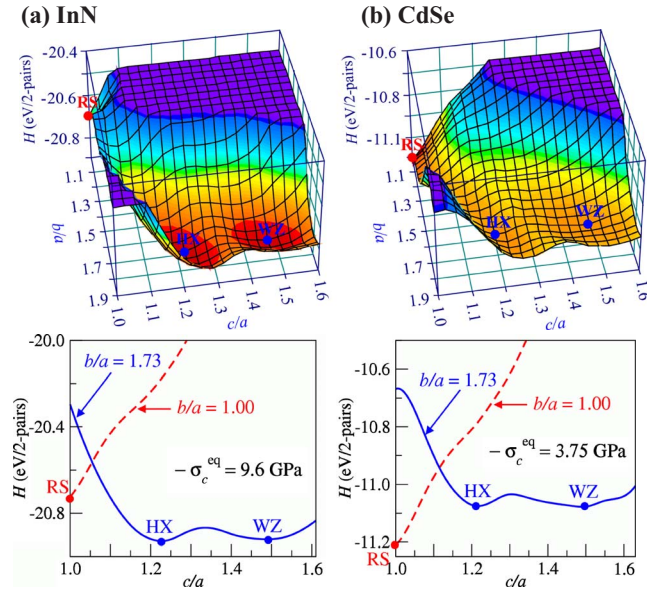


FIG. 9. (Color online) Enthalpy surface maps for (a) InN and (b) CdSe at their respective HX-WZ equilibrium c direction stress ($-\sigma_c^{\text{eq}}$). Their 2D sections for $b/a = 1.73$ (solid line) and 1.00 (dashed line) are also shown in the bottom panel. Note that, unlike other materials studied here, CdSe favors RS over HX phase under c -direction stress.

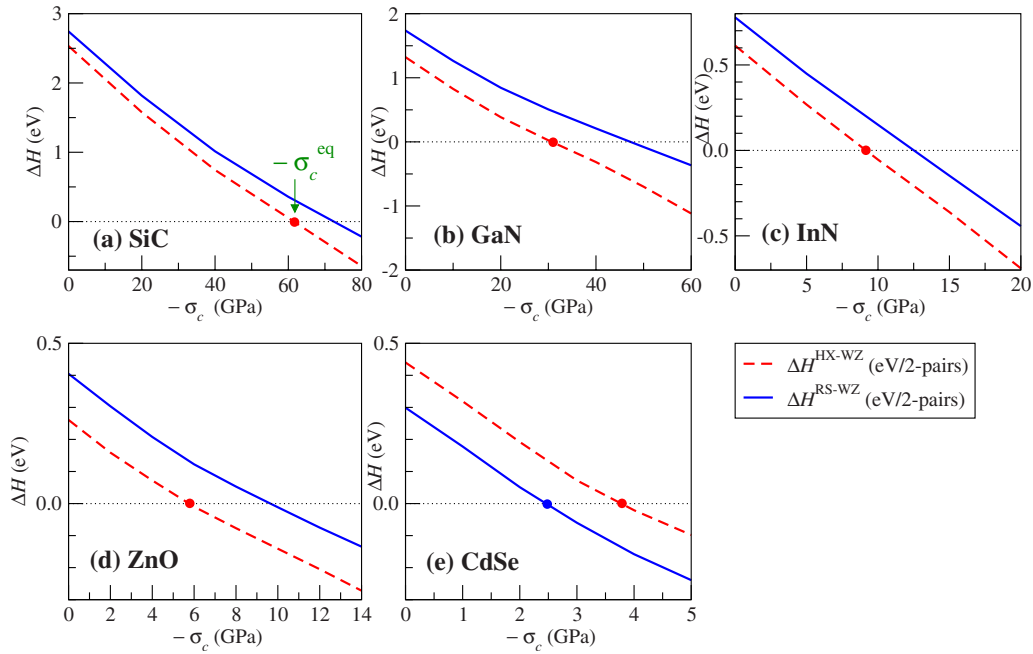


FIG. 10. (Color online) Enthalpy differences (ΔH) between the RS and WZ (solid line) and HX and WZ (dashed line) as a function of c -direction stress ($-\sigma_c$) for (a) SiC, (b) GaN, (c) InN, (d) ZnO, and (e) CdSe. As the magnitude of the stress reaches the equilibrium value ($-\sigma_c^{\text{eq}}$, indicated by solid dots), enthalpies of the HX and WZ structures become comparable. At stresses above $-\sigma_c^{\text{eq}}$, the HX phase is more stable.

tions have shown that under tensile loading, $[01\bar{1}0]$ -oriented ZnO nanowires can indeed transform into the HX structure under tensile loading.²⁸ The nanowires can sustain tensile stresses up to 14 GPa before failure, which is well above the equilibrium stress σ_b^{eq} predicted here. The equilibrium transformation stress of $\sigma_b^{\text{eq}}=5.8$ GPa for CdSe is the lowest among the materials studied. For nanostructures, other factors such as surface effects may contribute to facilitate the WZ \rightarrow HX transformation.³⁹ As a result, HX can emerge as

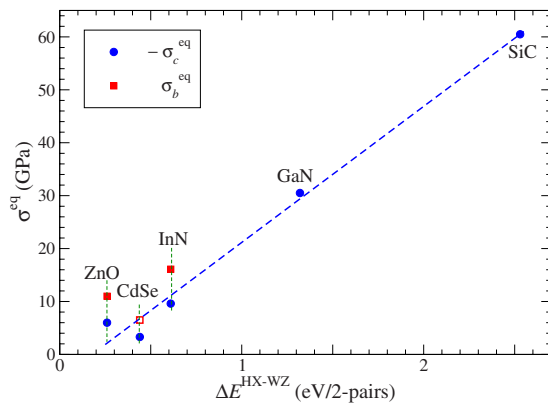


FIG. 11. (Color online) Correlation between equilibrium stresses ($-\sigma_c^{\text{eq}}$ and σ_b^{eq}) and the difference in energy (ΔE) between the HX and WZ phases for the five materials. $-\sigma_c^{\text{eq}}$ (σ_b^{eq}) is the equilibrium value of the c -direction compressive stress (b -direction tensile stress) for the HX and RS structures (see Table III). The energy difference $\Delta E=E^{\text{HX}}-E^{\text{WZ}}$ is calculated under conditions of zero external loading and is tabulated in Table II.

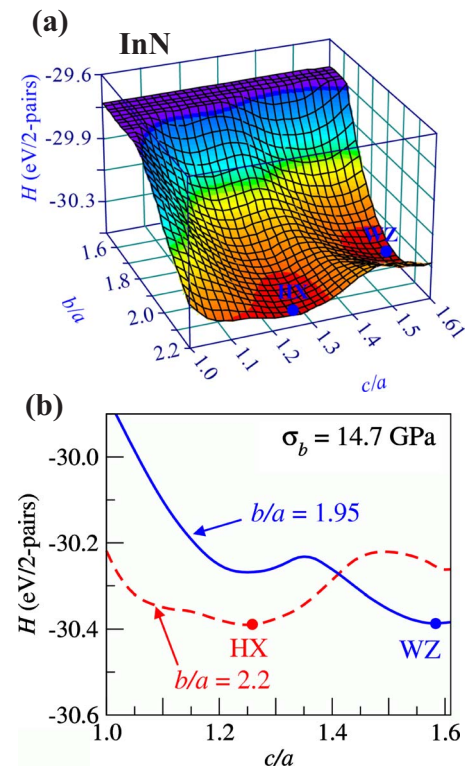


FIG. 12. (Color online) (a) Enthalpy surface maps (in eV/2-pairs) for InN at its HX-WZ stresses along the b direction, $\sigma_b^{\text{eq}}=14.7$ GPa. (b) 2D sections of the enthalpy surface for $b/a=1.95$ (solid line) and 2.20 (dashed line).

an intermediate phase during a WZ \rightarrow RS transformation in CdSe nanorods,³⁹ even though it does not have the lowest enthalpy in the bulk calculations. The relationship between σ_b^{eq} and $\Delta E^{\text{HX-WZ}} = E^{\text{HX}} - E^{\text{WZ}}$ is shown Fig. 11. Note that the σ_b^{eq} of CdSe may be higher than its fracture strength.

A local minimum for HX is not observed in the enthalpy surfaces for SiC and GaN, even at extremely high theoretical levels of σ_b (60 GPa for SiC and 30 GPa for GaN).³⁵ The lack of transformation in these materials can be attributed to the fact that their equilibrium transformation stresses are higher than their respective ultimate tensile strengths ($\sigma_b^{\text{eq}} \gg \sigma_{\text{UTS}}$). Indeed, EP-MD simulations have shown that for GaN nanowires, $\sigma_{\text{UTS}} \approx 30$ GPa,⁴⁰ only a fraction of the rough estimation of equilibrium stress of $\sigma_c^{\text{eq}} \geq 60$ GPa. The σ_b^{eq} of SiC is even higher since it has a higher energy difference between WZ and HX, making it more likely to have fractured before reaching its theoretical equilibrium stress of $\sigma_c^{\text{eq}} \geq 120$ GPa.

V. CONCLUSIONS

First principles calculations are carried out to study the stability of the WZ, RS, and HX phases of SiC, GaN, InN, ZnO, and CdSe under loading of different triaxialities. The energy of the materials correlates with their ionicity. At ambient conditions, WZ has the lowest energy level, HX has the second highest energy level, and RS has the highest energy level (with the exception of CdSe whose RS phase has a lower energy level than its HX phase). All five materials have the fourfold *wurtzite* structure as their stable and naturally occurring phase. Under all around hydrostatic compression, the materials can transform into the sixfold coordinated RS structure. Under uniaxial compression along the [0001] direction and uniaxial tension along the [01 $\bar{1}$ 0] direction, the materials can transform into the fivefold coordinated *unbuckled wurtzite* structure. The equilibrium conditions for the transformations are outlined. For the WZ \rightarrow RS transformation, the equilibrium hydrostatic pressures (p^{eq}) are predicted

to be 64.9, 44.1, 12.2, 8.2, and 2.2 GPa for SiC, GaN, InN, ZnO, and CdSe, respectively. These values are in good agreement with other theoretical calculations and experimental measurements. For the WZ \rightarrow HX transformation under uniaxial compression along the [0001] direction, the equilibrium stresses ($-\sigma_c^{\text{eq}}$) are 60.5, 30.5, 9.6, and 6.0 GPa for SiC, GaN, InN, and ZnO, respectively. For CdSe, uniaxial compression along the [0001] direction induces a WZ \rightarrow RS transformation at a stress of 2.4 GPa instead of the WZ \rightarrow HX transformation because the formation energy of RS is lower than HX for CdSe. For the WZ \rightarrow HX transformation under uniaxial tension along the [01 $\bar{1}$ 0] direction, the equilibrium transformation stresses (σ_b^{eq}) are 14.7, 10.8, and 5.8 GPa for InN, ZnO, and CdSe, respectively. The stress level for CdSe is close to its fracture limit. No transformation is observed for SiC and GaN under tension along the [01 $\bar{1}$ 0] direction due to the fact that their theoretical equilibrium transformation stresses are well above their respective ultimate fracture strengths. The magnitudes of p^{eq} , $-\sigma_c^{\text{eq}}$, and σ_b^{eq} are approximately linearly dependent with the formation energy differences between the relevant phase of the materials. Based on the calculations of five materials, we established a general linear function between p^{eq} and RS–WZ energy difference that could be useful for predicting the difference in formation energy of the RS and WZ phases of other materials when the equilibrium pressure is known or vice versa.

ACKNOWLEDGMENTS

This work was supported by NANOTEC (NN49-024) and Thailand Research Fund (BRG4880015 and PHD/0264/2545). A.J.K. and M.Z. are supported by NSF (CMS9984298) and NSFC (10528205). Computations are carried out at the National Synchrotron Research Center (Thailand) and at NAVO and ASC MSRCs through AFOSR MURI (D49620-02-1-0382).

APPENDIX

Tables IV–VIII.

TABLE IV. Lattice parameters for WZ, HX, and RS SiC under equilibrium loading conditions.

Parameters	WZ $p=0$ GPa	HX $-\sigma_c^{\text{eq}}=60.5$ GPa	RS $p^{\text{eq}}=64.9$ GPa
a (Å)	3.05 (3.06, ^a 3.08 ^b)	3.32	4.00 (3.68, ^{a,c} 3.84 ^d)
b (Å)	5.28	5.74	4.00
c (Å)	4.97	3.98	4.00
$V = \frac{abc}{2}$ (Å ³)	40.0	38.0	32.0
c/a	1.63	1.20	1.00
b/a	1.73	1.73	1.00
u	0.38	0.50	0.50
v	0.35	0.33	0.50

^aDFT (LDA) calculations by Karch *et al.* (Ref. 17).

^bXRD experiment by Schultz *et al.* (Ref. 47).

^cSynchrotron ADX by Yoshida *et al.* (Ref. 10).

^dDFT (LDA) calculations by Hatch *et al.* (Ref. 48).

TABLE V. Lattice parameters for WZ, HX, and RS GaN under equilibrium loading conditions.

Parameters	WZ	HX	RS
	$p=0$ GPa	$-\sigma_c^{\text{eq}}=30.5$ GPa	$p^{\text{eq}}=44.1$ GPa
a (Å)	3.15 (3.19, ^a 3.16, ^{b,c} 3.10 ^d)	3.43	4.16 (4.01, ^a 4.10, ^b 4.07 ^c)
b (Å)	5.46	5.94	4.16
c (Å)	5.11	4.12	4.16
$V=\frac{abc}{2}$ (Å ³)	44.0	42.0	36.0
c/a	1.62	1.20	1.00
b/a	1.73	1.73	1.00
u	0.38	0.50	0.50
v	0.35	0.33	0.50

^aSynchrotron EDX experiment by Xia *et al.* (Ref. 8).^bXRD experiment by Xie *et al.* (Ref. 49).^cDFT (LDA) calculations by Kim *et al.* (Ref. 50).^dDFT (LDA) calculations by Yeh *et al.* (Ref. 51).^eXRD experiment by Lada *et al.* (Ref. 52).

TABLE VI. Lattice parameters for WZ, HX, and RS InN under equilibrium loading conditions.

Parameters	WZ	HX		RS
	$p=0$ GPa	$-\sigma_c^{\text{eq}}=9.6$ GPa	$\sigma_b^{\text{eq}}=14.7$ GPa	$p^{\text{eq}}=12.2$ GPa
a (Å)	3.54 (3.53, ^a 3.54, ^{b,c} 3.52 ^d)	3.82	3.48	4.64 (4.67, ^e 4.62 ^d)
b (Å)	6.13	6.62	7.66	4.64
c (Å)	5.70	4.59	4.35	4.64
$V=\frac{abc}{2}$ (Å ³)	61.9	58.1	58.0	50.0
c/a	1.61	1.20	1.25	1.00
b/a	1.73	1.73	2.20	1.00
u	0.38	0.50	0.51	0.50
v	0.35	0.33	0.31	0.50

^aDFT (LDA) calculations by Kim *et al.* (Ref. 50).^bDFT (LDA) calculations by Yeh *et al.* (Ref. 51).^cXRD experiments by Osamura *et al.* (Ref. 53).^dDFT (LDA) calculations by Furthmüller *et al.* (Ref. 54).^eADX experiment by Ueno *et al.* (Ref. 6).

TABLE VII. Lattice parameters for WZ, HX, and RS ZnO under equilibrium loading conditions.

Parameters	WZ	HX		RS
	$p=0$ GPa	$-\sigma_c^{\text{eq}}=6.0$ GPa	$\sigma_b^{\text{eq}}=10.8$ GPa	$p^{\text{eq}}=8.2$ GPa
a (Å)	3.21 (3.20, ^a 3.25, ^{b,c} 3.26 ^d)	3.49	3.24	4.24 (4.28, ^b 4.27 ^{c,e})
b (Å)	5.54	6.03	6.46	4.24
c (Å)	5.15 (5.17, ^a 5.22 ^d)	4.19	4.20	4.24
$V=\frac{abc}{2}$ (Å ³)	45.7 (46.69, ^e 47.24, ^f 47.98 ^d)	44.1	44.0	38.1 (39.03, ^e 38.16 ^f)
c/a	1.61 (1.59 ^f)	1.20	1.30	1.00
b/a	1.73	1.73	2.00	1.00
u	0.38 (0.38 ^{a,d,f})	0.50	0.50	0.50
v	0.33	0.33	0.31	0.50

^aDFT (LDA) calculations by Malashevich and Vanderbilt (Ref. 56).^bSynchrotron EDX experiments by Desgrier (Ref. 5).^cXRD experiments by Karzel *et al.* (Ref. 55).^dEXAFS experiments by Decremps *et al.* (Ref. 57).^eDFT (GGA) calculations by Jaffe *et al.* (Ref. 16).^fDFT (GGA) calculations by Ahuja *et al.* (Ref. 45).

TABLE VIII. Lattice parameters for WZ, HX, and RS CdSe under equilibrium loading conditions.

Parameters	WZ $p=0$ GPa	HX		RS $p^{\text{eq}}=2.2$ GPa
		$-\sigma_c^{\text{eq}}=3.75$ GPa	$\sigma_b^{\text{eq}}=5.8$ GPa	
a (Å)	4.27 (4.30 ^a)	4.66	4.18	5.54 (5.58, ^a 5.71 ^b)
b (Å)	7.39	8.06	8.78	5.54
c (Å)	6.96	5.59	5.44	5.54
$V=\frac{abc}{2}$ (Å ³)	109.8	105.0	99.9	85.0
c/a	1.63	1.20	1.30	1.00
b/a	1.73	1.73	2.10	1.00
u	0.38	0.50	0.50	0.50
v	0.35	0.33	0.31	0.50

^aDFT calculations by Benkhetou *et al.* (Ref. 58).^bXRD experiment by Wickham *et al.* (Ref. 59).

- ¹C. T. Chan, D. Vanderbilt, S. G. Louie, and J. R. Chelikowsky, Phys. Rev. B **33**, 7941 (1986).
- ²S. Fahy, S. G. Louie, and M. L. Cohen, Phys. Rev. B **34**, 1191 (1986).
- ³A. Mujica, A. Rubio, A. Muñoz, and R. J. Needs, Rev. Mod. Phys. **75**, 863 (2003).
- ⁴C. F. Cline and D. R. Stephens, J. Appl. Phys. **36**, 2869 (1965).
- ⁵S. Desgreniers, Phys. Rev. B **58**, 14102 (1998).
- ⁶M. Ueno, M. Yoshida, A. Onodera, O. Shimomura, and K. Takemura, Phys. Rev. B **49**, 14 (1994).
- ⁷X. Wu, Z. Wu, L. Guo, C. Liu, J. Liu, X. Li, and H. Xu, Solid State Commun. **135**, 780 (2005).
- ⁸H. Xia, Q. Xia, and A. L. Ruoff, Phys. Rev. B **47**, 12925 (1993).
- ⁹Q. Xia, H. Xia, and A. L. Ruoff, Mod. Phys. Lett. B **8**, 345 (1994).
- ¹⁰M. Yoshida, A. Onodera, M. Ueno, K. Takemura, and O. Shimomura, Phys. Rev. B **48**, 10587 (1993).
- ¹¹C. H. Bates, W. B. White, and R. Roy, Science **137**, 993 (1962).
- ¹²J. Z. Jiang, J. S. Olsen, L. Gerward, D. Frost, D. Rubie, and J. Peyronneau, Europhys. Lett. **50**, 48 (2000).
- ¹³K. Kusaba, Y. Syono, and T. Kikegawa, Proc. Jpn. Acad., Ser. B: Phys. Biol. Sci. **75**, 1 (1999).
- ¹⁴N. E. Christensen and I. Gorczyca, Phys. Rev. B **50**, 4397 (1994).
- ¹⁵J. E. Jaffe and A. C. Hess, Phys. Rev. B **48**, 7903 (1993).
- ¹⁶J. E. Jaffe, J. A. Snyder, Z. Lin, and A. C. Hess, Phys. Rev. B **62**, 1660 (2000).
- ¹⁷K. Karch, F. Bechstedt, P. Pavone, and D. Strauch, Phys. Rev. B **53**, 13400 (1996).
- ¹⁸S. Limpijumng and S. Jungthawan, Phys. Rev. B **70**, 054104 (2004).
- ¹⁹S. Limpijumng and W. R. L. Lambrecht, Phys. Rev. B **63**, 104103 (2001).
- ²⁰S. Limpijumng and W. R. L. Lambrecht, Phys. Rev. Lett. **86**, 91 (2001).
- ²¹J. Serrano, A. H. Romero, F. J. Manjon, R. Lauck, M. Cardona, and A. Rubio, Phys. Rev. B **69**, 094306 (2004).
- ²²A. Zaoui and W. Sekkal, Phys. Rev. B **66**, 174106 (2002).
- ²³M. Côté, O. Zakharov, A. Rubio, and M. L. Cohen, Phys. Rev. B **55**, 13025 (1997).
- ²⁴F. Decremps, J. Pellicer-Porres, F. Datchi, J. P. Itie, A. Polian, F. Baudelet, and J. Z. Jiang, Appl. Phys. Lett. **81**, 4820 (2002).
- ²⁵S. Y. Bae, H. W. Seo, J. Park, H. Yang, J. C. Park, and S. Y. Lee, Appl. Phys. Lett. **81**, 126 (2002).
- ²⁶Z. W. Pan, Z. R. Dai, and Z. L. Wang, Science **291**, 1947 (2001).
- ²⁷A. J. Kulkarni, K. Sarasamak, S. Limpijumng, and M. Zhou, Philos. Mag. **87**, 2117 (2007).
- ²⁸A. J. Kulkarni, M. Zhou, K. Sarasamak, and S. Limpijumng, Phys. Rev. Lett. **97**, 105502 (2006).
- ²⁹L. Zhang and H. Huang, Appl. Phys. Lett. **89**, 183111 (2006).
- ³⁰L. Zhang and H. Huang, Appl. Phys. Lett. **90**, 023115 (2007).
- ³¹D. Vanderbilt, Phys. Rev. B **41**, 7892 (1990).
- ³²G. Kresse and J. Furthmüller, Comput. Mater. Sci. **6**, 15 (1996).
- ³³Here, we are interested only in the energy differences between phases. The calculations show that GGA consistently give slightly larger energy differences of between 0.1 and 0.4 eV/2 pairs (the largest case is for SiC which the energy difference by itself is large, i.e., 3 eV).
- ³⁴H. J. Monkhorst and J. D. Pack, Phys. Rev. B **13**, 5188 (1976).
- ³⁵See EPAPS Document No. E-PRBMDO-77-026802 for additional enthalpy surface maps. For more information on EPAPS, see <http://www.aip.org/pubservs/epaps.html>.
- ³⁶For some low pressure or low stress loading conditions, the enthalpy surface (or energy surface for the stress-free case) might not have a local minimum near the HX structure. In such cases, the c/a and b/a defining the enthalpy of the HX phase is taken from the first (meta)stable HX when the pressure and/or stress is increased.
- ³⁷J. C. Phillips, Rev. Mod. Phys. **42**, 317 (1970).
- ³⁸M. S. Miao and W. R. L. Lambrecht, Phys. Rev. B **68**, 092103 (2003).
- ³⁹M. Grunwald, E. Rabani, and C. Dellago, Phys. Rev. Lett. **96**, 255701 (2006).
- ⁴⁰Z. Wang, X. Zu, L. Yang, F. Gao, and W. J. Weber, Phys. Rev. B **76**, 045310 (2007).

- ⁴¹M. S. Miao and W. R. L. Lambrecht, *Phys. Rev. B* **68**, 092103 (2003).
- ⁴²K. J. Chang and M. L. Cohen, *Phys. Rev. B* **35**, 8196 (1987).
- ⁴³M. Catti, *Phys. Rev. Lett.* **87**, 035504 (2001).
- ⁴⁴J. Serrano, A. Rubio, E. Hernandez, A. Munoz, and A. Mujica, *Phys. Rev. B* **62**, 16612 (2000).
- ⁴⁵R. Ahuja, L. Fast, O. Eriksson, J. M. Wills, and B. Johansson, *J. Appl. Phys.* **83**, 8065 (1998).
- ⁴⁶J. M. Recio, M. A. Blanco, V. Luana, R. Pandey, L. Gerward, and J. S. Olsen, *Phys. Rev. B* **58**, 8949 (1998).
- ⁴⁷H. Schulz and K. H. Thiemann, *Solid State Commun.* **32**, 783 (1979).
- ⁴⁸D. Hatch, H. T. Stokes, J. Dong, J. Gunter, H. Wang, and J. Lewis, *Phys. Rev. B* **71**, 184109 (2005).
- ⁴⁹Y. Xie, Y. Qian, S. Zhang, W. Wang, X. Liu, and Y. Zhang, *Appl. Phys. Lett.* **69**, 334 (1996).
- ⁵⁰K. Kim, W. R. L. Lambrecht, and B. Segall, *Phys. Rev. B* **53**, 16310 (1996).
- ⁵¹C. Y. Yeh, Z. W. Lu, S. Froyen, and A. Zunger, *Phys. Rev. B* **46**, 10086 (1992).
- ⁵²M. Lada, A. G. Cullis, P. J. Parbrook, and M. Hopkinson, *Appl. Phys. Lett.* **83**, 2808 (2003).
- ⁵³K. Osamura, S. Naka, and Y. Murakami, *J. Appl. Phys.* **46**, 3432 (1975).
- ⁵⁴J. Furthmuller, P. H. Hahn, F. Fuchs, and F. Bechstedt, *Phys. Rev. B* **72**, 205106 (2005).
- ⁵⁵H. Karzel, W. Potzel, M. Kofferlein, W. Schiessl, M. Steiner, U. Hiller, G. M. Kalvius, D. W. Mitchell, T. P. Das, P. Blaha, K. Schwarz, and M. P. Pasternak, *Phys. Rev. B* **53**, 11425 (1996).
- ⁵⁶A. Malashevich and D. Vanderbilt, *Phys. Rev. B* **75**, 045106 (2007).
- ⁵⁷F. Decremps, F. Datchi, A. M. Saitta, A. Polian, S. Pascarelli, A. D. Cicco, J. P. Itie, and F. Baudlet, *Phys. Rev. B* **68**, 104101 (2003).
- ⁵⁸N. Benkhetto, D. Rached, B. Soudini, and M. Driz, *Phys. Status Solidi B* **241**, 101 (2004).
- ⁵⁹J. N. Wickham, A. B. Herhold, and A. P. Alivisatos, *Phys. Rev. Lett.* **84**, 923 (2000).